CHAPTER

2

High-mobility wireless channels

OUTLINE

Chapter points

- Wireless channel models for high mobility environments: multipath and Doppler shifts.
- Three domains to represent the channels: frequency-time, delay-time, and delay-Doppler.
- Statistical channel models.

To know what you know and what you do not know, that is true knowledge.
Confucius

Any transmitted signal undergoes variations as it propagates through the wireless channel. Several factors, including channel propagation prop-

https://doi.org/10.1016/B978-0-32-385028-5.00010-4

erties and obstacles in a propagation path, can cause fluctuations in received signal strength, commonly termed fading. Fading can be broadly classified as large-scale fading and small-scale fading.

Large-scale fading involves variations of the average received signal strength due to signal propagation over long distances (over several hundred meters) and a complete or partial line of sight (LoS) path loss due to shadowing caused by the presence of large obstacles in the propagation path.

Small-scale fading, on the other hand, refers to rapid fluctuations that occur within a short period (of the order of seconds) or over short distances (of the order of meters). These fluctuations arise due to constructive and destructive superposition of the transmitted signal echoes that arrive through different propagation paths, a phenomenon known as multipath propagation.

This chapter will focus on small-scale fading, since the physical layer design of a communications system is based on combating the small-scale fading of a wireless channel. As we are concerned with delay-Doppler communications, it is essential to have an in-depth understanding of the delay-Doppler domain representation of a channel before diving into the more practical aspects of transceiver design in later chapters. The delay-Doppler domain has close resemblance with the physical geometric parameters of the environment such as the distance and relative velocity of the reflectors. Under the practical assumption that there are a limited number of reflectors in the vicinity of the receiver, the delay-Doppler domain offers a more compact representation of the geometric channel, as compared to the traditional delay-time or frequency-time domains.

2.1 Input–output model of the wireless channel

Consider the transmission of a signal over a wireless channel. At the transmitter, a baseband signal $s(t)$ of bandwidth B is up-converted to a passband $[f_c - B/2, f_c + B/2]$, where f_c is the carrier frequency used for transmission. At the receiver, the received signal is down-converted to the baseband equivalent signal, denoted by $r(t)$. Since most of the receiver processing, such as demodulation, decoding, and detection, occurs at baseband, we will focus only on the baseband equivalent representation of wireless channels. With the final aim of arriving at the delay-Doppler representation of the channel, we start with the geometric model of a wireless channel.

2.1.1 Geometric model

Geometric models are based on the ray-tracing technique, which is an easy and useful tool to understand how the transmitted waves interfere

with the physical channel. In order to derive a deterministic model of the wireless channel, we start with the ray-tracing technique and use the knowledge of the physical geometry of the propagation environment. Due to multipath propagation, the received signal $r(t)$ is an aggregation of delayed, Doppler shifted, and attenuated copies of the transmitted signal $s(t)$. The delay is a function of the length of each propagation path, whereas Doppler shift occurs due to the relative motion in the scene of transmitter, receiver, and reflectors.

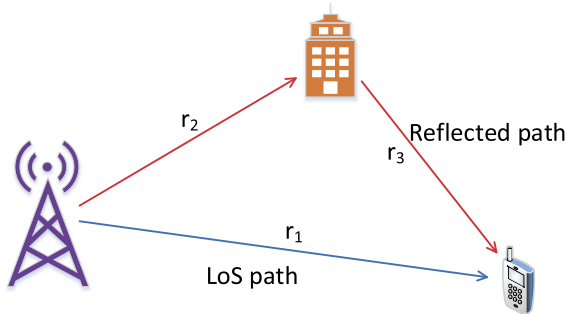

FIGURE 2.1 Paths with different propagation delays.

Let us first consider a simple wireless channel shown in Fig. 2.1, where the transmitter (base-station), the receiver (mobile), and the reflector (building) are static. Since there is no relative motion in the scene, the transmitted signal does not undergo any Doppler shift. However, the difference in the propagation delay of the direct and reflected paths causes two copies of $s(t)$ to arrive at the mobile receiver at different times. The direct path from the base-station to the mobile incurs a propagation delay due to distance r_1. On the other hand, the path reflected from the building has to travel a combined distance of $r_2 + r_3$. Assume that the direct and reflected paths have a baseband equivalent complex gain (attenuation) of g_1 and g_2, respectively. Using the superposition principle, the received signal $r(t)$ can be expressed as

$$r(t) = g_1 s(t - \tau_1) + g_2 s(t - \tau_2), \tag{2.1}$$

where $\tau_1 = r_1/c$ is the delay of the LoS path, $\tau_2 = (r_2 + r_3)/c$ is the delay of the reflected path, and $c = 3 \cdot 10^8$ m/s is the speed of light. The difference in propagation delays $\tau_2 - \tau_1$ is known as the *delay spread*.

In the case of a channel with more than two paths, the delay spread is defined as the difference between the propagation delays of the longest and shortest paths, i.e., $\tau_{\max} - \tau_{\min}$.

Now consider the case in Fig. 2.2, where the mobile receiver is in a car which is moving towards the base-station with a relative velocity v. We

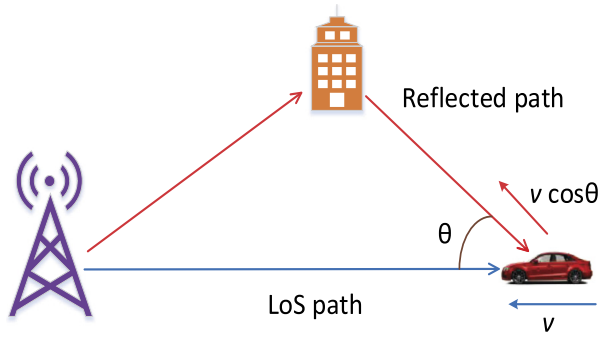

FIGURE 2.2 Paths with different Doppler shifts due to the different angles of arrival.

assume that the bandwidth B of $s(t)$ is very small compared to the carrier frequency f_c, i.e., $f_c \gg B$. The Doppler shift due to a relative velocity υ is given by $\frac{\upsilon}{c} f_c$. The received signal can then be expressed as the sum of delayed and Doppler shifted copies of the transmitted signal as

$$r(t) = \underbrace{g_1 e^{j2\pi \nu_1 (t-\tau_1)}}_{g(\tau_1,t)} s(t-\tau_1) + \underbrace{g_2 e^{j2\pi \nu_2 (t-\tau_2)}}_{g(\tau_2,t)} s(t-\tau_2), \tag{2.2}$$

where $\nu_1 = \frac{\upsilon}{c} f_c$ is the Doppler shift of the LoS path, $\nu_2 = \frac{\upsilon \cos\theta}{c} f_c$ is the Doppler shift of the reflected path, $|\nu_2 - \nu_1|$ is the *Doppler spread*, and the time-dependent functions

$$g(\tau_i, t) = g_i e^{j2\pi \nu_i (t-\tau_i)}, \quad i = 1, 2, \tag{2.3}$$

represent the time-varying attenuation of the propagation paths incurred by delay and Doppler shifts. The delay spread ($\tau_{\max}$) and Doppler spread ($\nu_{\max}$) values for some typical wireless channels are listed in Table 2.1.

In general, the multipath fading channel in (2.3) can then be modeled as an LTI system of the form

$$\boxed{r(t) = \int_0^\infty g(\tau, t) s(t-\tau) d\tau,} \tag{2.4}$$

where $g(\tau, t)$ is the delay-time impulse response of the channel and $0 \leq \tau < \infty$ represents the propagation delay.

The time-frequency impulse response of the channel at a fixed time t can be obtained by taking a Fourier transform along the delay dimension of $g(\tau, t)$,

$$\boxed{H(f, t) = \int_\tau g(\tau, t) e^{-j2\pi f \tau} d\tau.} \tag{2.5}$$

TABLE 2.1 Delay spread ($\tau_{\max}$) and Doppler spread ($\nu_{\max}$) for some typical wireless channels.

$\Delta r_{\max}$	Indoor (3 m)	Outdoor (3 km)
$\tau_{\max}$	10 ns	10 μs

$v_{\max}$	$f_c = 2$ GHz	$f_c = 60$ GHz
$v = 1.5$ m/s $= 5.5$ km/h	$\nu_{\max} = 10$ Hz	$\nu_{\max} = 300$ Hz
$v = 3$ m/s $= 11$ km/h	$\nu_{\max} = 20$ Hz	$\nu_{\max} = 600$ Hz
$v = 30$ m/s $= 110$ km/h	$\nu_{\max} = 200$ Hz	$\nu_{\max} = 6$ kHz
$v = 150$ m/s $= 550$ km/h	$\nu_{\max} = 1$ kHz	$\nu_{\max} = 30$ kHz

For the general case, where the channel has P paths, each with the gain g_i, the delay τ_i, and the Doppler shift ν_i, $i = 1, \ldots, P$, substituting $g(\tau_i, t)$ in (2.2) into the above equation yields the frequency response as

$$H(f,t) = \sum_{i=1}^{P} g_i \mathrm{e}^{-j2\pi\nu_i\tau_i} \mathrm{e}^{-j2\pi(f\tau_i - \nu_i t)}. \tag{2.6}$$

In practice, $H(f,t)$ is assumed to be a slowly time-varying function of t. For the special case of a static channel, i.e., $\nu_i = 0, \forall i$, $H(f,t)$ reduces to the time-independent frequency response $H(f)$.

2.1.2 Delay-Doppler representation

We have shown how the different delayed and Doppler shifted components lead to the received signal $r(t)$ and define a model for the wireless channel response. However, the effect of Doppler shift is not immediately evident in the delay-time response $g(\tau, t)$ that we have obtained in the last section. The effect of a scatterer can be represented using the delay (due to distance) and Doppler shift (due to relative motion) undergone by the transmitted signal $s(t)$ that bounces off it. This enables a linear time-varying wireless channel to be completely characterized by the delay-Doppler parameters of the scatterers in the vicinity of the receiver. Since the delay-Doppler response more closely resembles the physical wireless channel, it is useful to have a delay-Doppler representation of the channel.

In general, the small-scale fading effects of a wireless channel can be represented using a small number of scatterers in the vicinity of the receiver. This means that the wireless channel has a sparse representation in the delay-Doppler domain. In order to illustrate this explicitly, let us consider a wireless channel with P propagation paths with distinct delay and Doppler shift parameters.

The two-path input-output relation given in (2.2) can be generalized for a number P of propagation paths as

$$r(t) = \sum_{i=1}^{P} g_i e^{j2\pi\nu_i(t-\tau_i)} s(t-\tau_i), \tag{2.7}$$

where g_i is the path gain and τ_i and ν_i are the delay and Doppler shift, respectively, associated with the i-th path, $i = 1, \ldots, P$.

We define the delay-Doppler response as

$$h(\tau, \nu) = \sum_{i=1}^{P} g_i e^{-j2\pi\nu_i\tau_i} \delta(\tau-\tau_i)\delta(\nu-\nu_i), \tag{2.8}$$

which is a sparse representation of the wireless channel in the delay-Doppler domain due to the limited number of paths P. Then the received signal $r(t)$ can be written as

$$r(t) = \int\int h(\tau, \nu) e^{j2\pi\nu t} s(t-\tau) d\nu d\tau. \tag{2.9}$$

From (2.8), we see that the channel in the delay-Doppler domain is completely represented by the parameters (g_i, τ_i, ν_i) for $i = 1, \ldots, P$. Note that the term $e^{-j2\pi\nu_i\tau_i}$ is a constant phase shift that may be absorbed into the channel coefficient g_i with a slight abuse of notation. Without loss of generality, in the following we will simply assume:

$$\boxed{h(\tau, \nu) = \sum_{i=1}^{P} g_i \delta(\tau-\tau_i)\delta(\nu-\nu_i).} \tag{2.10}$$

Figs. 2.3(a) and 2.3(b) show a simple delay-Doppler representation of the channel between the base-station (Tx) and a vehicle (Rx) on a highway. Both these pictures were taken 100 ms apart in time. Note that the transmitted signal duration is in general less than 10 ms, which is much shorter than the geometric coherence time, i.e., the duration over which physical geometry of the channel can be considered to be invariant. This allows the channel to have a roughly time-invariant response to an impulse in the delay-Doppler domain as long as the impulse is transmitted within the geometric coherence time. The knowledge of the geometric coherence time is crucial in designing the transmission parameters such as signal duration according to the specific channel parameters such as delay spread and Doppler spread.

As an example of a high mobility scenario, consider Figs. 2.3(a) and 2.3(b), where a base-station transmits to a receiver traveling at nearly

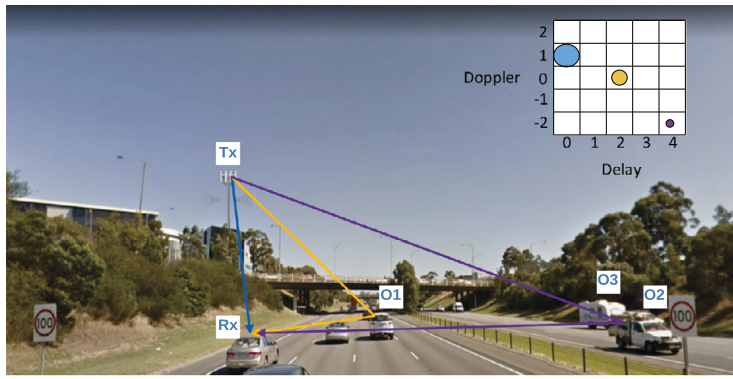

(a) Scenario 1

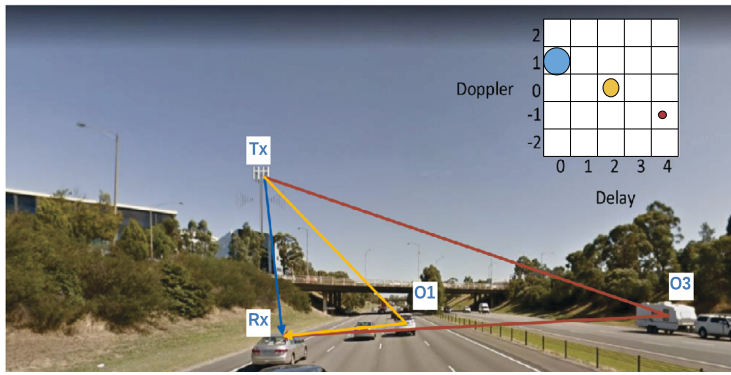

(b) Scenario 2

FIGURE 2.3 An example of high-mobility wireless channel scenarios showing how the delay-Doppler channel response changes when the geometry of the scene changes.

100 km/h in a car. Due to the presence of scatterers, Rx receives an aggregation of P delay and Doppler shifted echoes of the transmitted signal. The scatterers considered in this example are labeled as O1, O2, and O3. The delay-Doppler grid in the figure shows what the mobile user receives if a dot at delay and Doppler position $[0, 0]$ is transmitted. Each colored dot in the delay-Doppler grid corresponds to the propagation path denoted by the same colored ray. The area of the dot in the delay-Doppler grid denotes the gain of each propagation path. Assume that each integer value along the delay and Doppler axis corresponds to a reflector at a distance of 10 m and a speed of 50 km/h relative to Rx. For example, the blue (black in print version) dot corresponds to a reflector traveling at 50 km/h (corresponding to the integer Doppler tap 1) relative to the receiver Rx.

The largest dot in Fig. 2.3(a) corresponds to the LoS path between the base-station and the receiver vehicle Rx, shown by the blue (black in print

version) colored ray. It is assigned a delay of 0, being the signal that arrives first, and has a positive Doppler shift, as the car is moving towards the base-station. The yellow (light gray in print version) circle corresponds to the path that is reflected off another vehicle (O1) traveling along the same direction as Rx in the highway, but with lower speed compared to Rx relative to the base-station. The smallest circle corresponds to the longest path due to the reflection from (O2) denoted by the purple (dark gray in print version) dot and rays. The Doppler shift has a negative value as the vehicle is moving away from the base-station and its relative velocity with respect to Rx is zero at this instant due to the relative angles between the vehicles. The reflection from vehicle O3 is ignored due to severe path attenuation as the transmitted wave has to travel a much longer distance than in the case of O2.

Let us now discuss how the channel, and hence the delay-Doppler representation, remains roughly invariant in short intervals of time. As shown in Fig. 2.3(b), in the space of 100 ms, vehicle O2 has moved farther away from Rx and O3 has moved closer to Rx. This causes the reflected wave off O3 (as denoted by the red (mid gray in print version) dot) to be stronger than the one off O2. The Doppler shift due to O3 is less than that due to O2 as O3 is traveling at almost half the speed of O2.

The key conclusion to be drawn from this example is that by aptly designing the frame duration, the delay-Doppler representation of a typical wireless channel can be made to be roughly time-invariant for the duration of a signal frame.

2.2 Continuous-time baseband channel model

In the previous sections, we have looked at general representations of a wireless channel. For a receiver that operates with limited delay and Doppler resolution, it is impossible to observe the true channel parameters. The observed channel is a function of the true channel as well as the delay and Doppler resolution of the receiver. Therefore we start with a continuous-time baseband representation of the channel from the receiver's point of view. Then, we will look at how the receiver sampling results in a discrete-time equivalent baseband channel. In Chapter 4, we will analyze in detail the discrete delay-Doppler channel when a digital receiver is used.

Let the transmitted signal $s(t)$ be of bandwidth $M\Delta f$ [Hz] and duration NT [s]. Consider a baseband equivalent channel model with P propagation paths. For the i-th path, $i = 1, \ldots, P$, the complex path gain is g_i, and the actual delay and Doppler shift are τ_i and ν_i, respectively, given by

$$\tau_i = \frac{\ell_i}{M\Delta f} \leq \tau_{\max} = \frac{\ell_{\max}}{M\Delta f} \quad \nu_i = \frac{\kappa_i}{NT} \text{ with } |\nu_i| \leq \nu_{\max}, \tag{2.11}$$

where $\ell_i, \kappa_i \in \mathbb{R}$ are the *normalized delay* and *normalized Doppler shift*, respectively, and $\ell_{\max} \in \mathbb{R}$ is the *normalized delay* associated with $\tau_{\max}$.

We assume that the channel is *underspread*, i.e., $\tau_{\max} \nu_{\max} \ll 1$ and $T\Delta f = 1$. Under the underspread assumption, we have $\ell_{\max} < M$ and the normalized Doppler shifts $-N/2 < \kappa_i < N/2$. Recalling from the previous sections, since the number of channel coefficients P in the delay-Doppler domain is typically limited, the delay-Doppler channel response has a sparse representation:

$$h(\tau, \nu) = \sum_{i=1}^{P} g_i \delta(\tau - \tau_i)\delta(\nu - \nu_i). \tag{2.12}$$

We let $\mathcal{L} = \{\ell_i\}$ of size $|\mathcal{L}|$ be the set of distinct *normalized delays* among the P paths in the delay-Doppler domain, we let $\mathcal{K}_\ell = \{\kappa_i \mid \ell = \ell_i\}$ be the set of *normalized Doppler shifts* for each path with normalized delay ℓ_i, and we let

$$v_\ell(\kappa) = \begin{cases} g_i, & \text{if } \ell = \ell_i \text{ and } \kappa = \kappa_i, \\ 0, & \text{otherwise} \end{cases} \tag{2.13}$$

be the *Doppler response* at delay ℓ. Then we can rewrite (2.12) as

$$h(\tau, \nu) = \sum_{\ell \in \mathcal{L}} \sum_{\kappa \in \mathcal{K}_\ell} v_\ell(\kappa)\delta(\tau - \ell T/M)\delta(\nu - \kappa \Delta f/N). \tag{2.14}$$

Note that the continuous delay-time channel response is given by

$$\boxed{g(\tau, t) = \int_\nu h(\tau, \nu) \mathrm{e}^{j2\pi\nu(t-\tau)}\, d\nu.} \tag{2.15}$$

Substituting (2.14) into (2.15) yields the corresponding delay-time channel response, for all $\ell \in \mathcal{L}$, as

$$g(\tau, t) = \sum_{\ell \in \mathcal{L}} \sum_{\kappa \in \mathcal{K}_\ell} v_\ell(\kappa) \mathrm{e}^{j2\pi\kappa \frac{\Delta f}{N}(t-\ell T/M)} \delta(\tau - \ell T/M). \tag{2.16}$$

Evaluating (2.16) at $\tau = \ell T/M$ for all $\ell \in \mathcal{L}$ yields

$$g(\tau = \ell T/M, t) = \sum_{\kappa \in \mathcal{K}_\ell} v_\ell(\kappa) \mathrm{e}^{j2\pi\kappa \frac{\Delta f}{N}(t-\ell T/M)}. \tag{2.17}$$

In the special case of a static channel with no Doppler spread, i.e., $\kappa = 0$, (2.16) reduces to

$$g(\tau = \ell T/M, t) = v_\ell(0). \tag{2.18}$$

2.3 Discrete-time baseband channel model

In the previous section, we have looked at the continuous-time channel model. When modeling a bandpass communication system, it is convenient to work with a discrete baseband equivalent representation of the system. At the transmitter, a signal of bandwidth $B = M\Delta f$ is up-converted to a carrier frequency f_c to occupy a bandpass channel, assuming $f_c \gg B$. At the receiver, the channel impaired signal is down-converted to baseband and sampled at $f_s = B = M\Delta f$ Hz, yielding NM complex samples per frame of duration NT [s].

By sampling the received waveform $r(t)$ at $t = qT/M$, where $q = 0, \ldots, NM-1$, and discretizing delay variable $\tau = lT/M$ for $l = 0, \ldots, M-1$, we have the discrete baseband delay-time channel response in (2.16) as

$$g^{\mathrm{s}}[l,q] = g(lT/M, qT/M) = \sum_{\ell\in\mathcal{L}} \left(\sum_{\kappa\in\mathcal{K}_\ell} \nu_\ell(\kappa) z^{\kappa(q-l)} \right) \mathrm{sinc}(l-\ell), \qquad (2.19)$$

where $\mathrm{sinc}(x) = \sin(\pi x)/(\pi x)$ and $z = \mathrm{e}^{\frac{j2\pi}{NM}}$. Thus the discrete delay-time input-output relation is given as

$$r[q] = r(qT/M) = \sum_{l=0}^{M-1} g^{\mathrm{s}}[l,q]\, s[q-l]. \qquad (2.20)$$

Note that due to fractional delays, the sampling at the receiver introduces interference between Doppler responses at different delays. This is due to sinc reconstruction of the delay-time response at fractional delay points ($\ell \in \mathcal{L}$). However, in typical wideband systems, the channel path delays can be approximated to integer multiples of T/M, without loss of accuracy, i.e., $\ell = l \in \mathbb{Z}$, and the sinc function in (2.19) reduces to

$$\mathrm{sinc}(l-\ell) = \begin{cases} 1, & \text{if } \ell = l, \\ 0, & \text{otherwise.} \end{cases} \qquad (2.21)$$

Consequently, the relation between the actual Doppler response and the sampled time domain channel at each integer delay tap $l \in \mathcal{L}$ in (2.19) reduces to

$$g^{\mathrm{s}}[l,q] = \begin{cases} \sum_{\kappa\in\mathcal{K}_l} \nu_l(\kappa) z^{\kappa(q-l)} & \text{for } \ell = l \in \mathcal{L}, \\ 0 & \text{otherwise.} \end{cases} \qquad (2.22)$$

Here, we remind the reader that the effective channel as seen by the receiver depends on the actual channel response as well as the operation parameters (delay resolution) of the receiver. Further, we denote $l_{\max} = \max(\mathcal{L})$ to be the *maximum channel delay tap*.

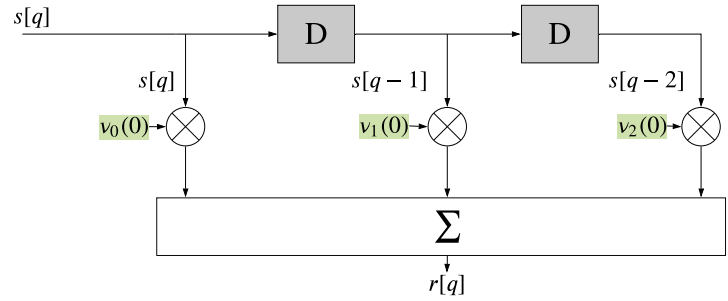

(a) Linear time-invariant channel

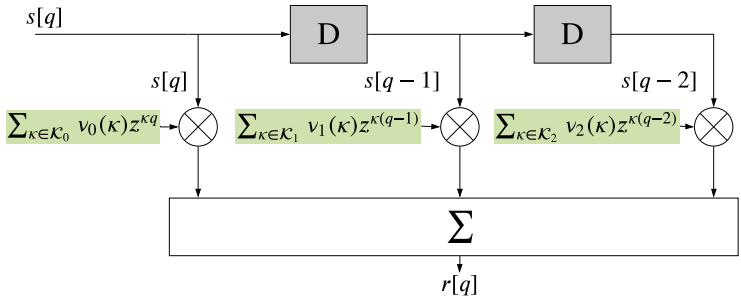

(b) Linear time-varying channel

FIGURE 2.4 The TDL models for static and high-mobility channels with integer delay taps $\mathcal{L} = \{0, 1, 2\}$.

Fig. 2.4 shows the delay-time channel for static and mobile channels, respectively, represented using a tapped delay line (TDL) model for the set of integer delay taps $\mathcal{L} = \{0, 1, 2\}$. For the static case in Fig. 2.4(a), the channel tap corresponding to each delay tap l remains constant since from (2.18) $\nu_l(\kappa) = 0$ for $\kappa \neq 0$. However, for the time-variant channel case in Fig. 2.4(b), each delay tap coefficient is the sum of distinct Doppler paths within the same delay tap, each affected by a time-varying phase rotation.

2.4 Relation among different channel representations

From previous sections, when $s(t)$ is the transmitted time domain signal, the received signal $r(t)$ in the presence of time-variant multipath channel (also known as doubly dispersive channel) can be written as

$$r(t) = \int_{\tau} g(\tau, t) s(t - \tau) d\tau \tag{2.23}$$

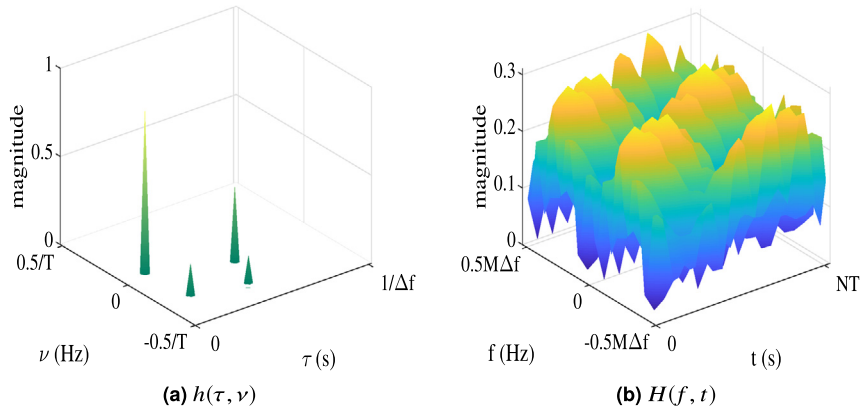

FIGURE 2.5 The continuous delay-Doppler vs time-frequency channel representation of a high-mobility multipath channel (linear time-varying).

$$= \int_f H(f,t)S(f)e^{j2\pi ft}df \tag{2.24}$$

$$= \int_\nu \int_\tau h(\tau,\nu)s(t-\tau)e^{j2\pi\nu t}d\tau d\nu, \tag{2.25}$$

where $S(f)$ is the Fourier transform of $s(t)$.

The three equivalent relations in (2.23)–(2.25) can be interpreted as follows. The channel $g(\tau,t)$ in (2.23) represents the time-varying impulse response and the relation can be seen as a straightforward generalization of the LTI system. The relation in (2.24) describes the time-frequency channel and an OFDM-based system is defined by this relation. Finally, the relation in (2.25) describes the delay-Doppler channel and an OTFS system is based on this relation.

Now, the relation between the time-frequency ($H(f,t)$) and delay–Doppler ($h(\tau,\nu)$) channel responses can be given by a pair of two-dimensional symplectic Fourier transforms (SFTs) as

$$\boxed{h(\tau,\nu) = \text{SFT}\{H(f,t)\} = \iint H(f,t)e^{-j2\pi(\nu t - f\tau)}dtdf,} \tag{2.26}$$

$$\boxed{H(f,t) = \text{ISFT}\{h(\tau,\nu)\} = \iint h(\tau,\nu)e^{j2\pi(\nu t - f\tau)}d\tau d\nu,} \tag{2.27}$$

where (2.26) and (2.27) define the SFT and ISFT operations, respectively.

Figs. 2.5 and 2.6 illustrate the sparsity of the delay-Doppler channel response in comparison with the time-frequency channel response of linear time-varying and time-invariant channels. The nonzero coefficients in the

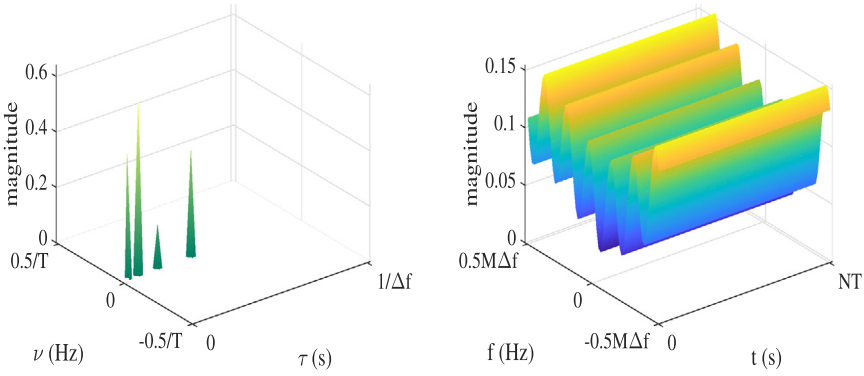

FIGURE 2.6 The continuous delay-Doppler vs. time-frequency channel representation of a static multipath channel (linear time-invariant).

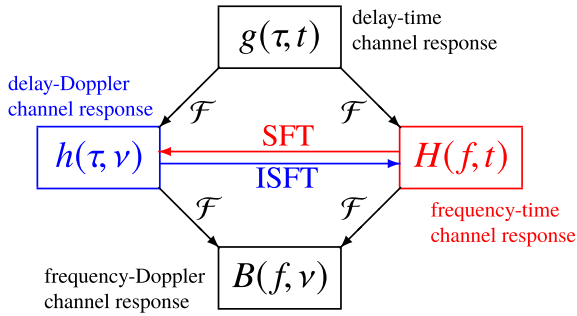

FIGURE 2.7 Different domain representations of a time-variant multipath channel impulse response $g(\tau, t)$, also denoted as the delay-time channel response.

delay-Doppler plane at location (τ, ν) represent the magnitude of the propagation gain of a path with the corresponding delay and Doppler shift. The number of paths in this case is set to $P = 4$. It can be observed that the corresponding frequency-time channel in Fig. 2.5 is time-varying and hence requires more time-frequency coefficients to accurately represent the channel. However, for a static channel, the frequency-time channel is time-invariant with P paths as shown in Fig. 2.6. As seen by the delay-Doppler representation, all the paths have Doppler shift $\nu_i = 0$, where $i = 1, \ldots, P$. Fig. 2.6 represents a frequency selective channel, whereas Fig. 2.5 is both time and frequency selective, or in other words, doubly selective.

In summary, Fig. 2.7 illustrates the relations between the four equivalent time-variant multipath channels defined in the literature, where $\mathcal{F}$

denotes the Fourier operation and $B(f, \nu)$ denotes the Doppler-variant frequency response.

2.5 Channel models for numerical simulations

We adopt the tapped delay line model of the wireless channel shown in Fig. 2.4(b) for our simulations. The channel gain g_i is modeled as a circular symmetric Gaussian complex random variable[1] independent across all paths for $i = 1, \ldots P$, whose envelope is Rayleigh distributed with variance σ_i^2. In general, the channel characteristics can be specified using the power delay profile and maximum Doppler spread of the propagation environment.

2.5.1 Standard wireless mobile multipath propagation scenarios

Here, we list some standard 3GPP multipath fading channel profiles, which will be used to generate channel models for simulations in later chapters. The fading models listed here represent low, medium, and high delay spread environments. The power delay profiles are given in Tables 2.2, 2.3, 2.4.

TABLE 2.2 Extended Pedestrian A (EPA) model.

Excess tap delay (ns)	0	30	70	90	110	190	410
Relative power (dB)	0.0	−1.0	−2.0	−3.0	−8.0	−17.2	−20.8

TABLE 2.3 Extended Vehicular A (EVA) model.

Excess tap delay (ns)	0	30	150	310	370	710	1090	1730	2510
Relative power (dB)	0.0	−1.5	−1.4	−3.6	−0.6	−9.1	−7.0	−12.0	−16.9

TABLE 2.4 Extended Typical Urban (ETU) model.

Excess tap delay (ns)	0	50	120	200	230	500	1600	2300	5000
Relative power (dB)	−1.0	−1.0	−1.0	0.0	0.0	0.0	−3.0	−5.0	−7.0

Let $\nu_{\max} = f_c u_{\max}/c$ be the maximum Doppler shift of the overall multipath channel. We assume a single Doppler shift is associated with the i-th delay path and follows the classic Jakes spectrum, i.e., $\nu_i = \nu_{\max} \cos(\theta_i)$, where θ_i is uniformly distributed over $[-\pi, \pi]$. The MATLAB® code for

[1] The complex channel gain is $g_i = a_i + jb_i$, where a_i and b_i are zero-mean, independent and identically distributed Gaussian random variables with variance $\frac{\sigma_i^2}{2}$, i.e., $a_i, b_i \sim \mathcal{N}(0, \frac{\sigma_i^2}{2})$.

generating the delay-Doppler channel coefficients for a particular UE speed $u_{\max}$ is given in MATLAB code 6 in Appendix C.

2.5.2 Synthetic propagation scenario

For the purpose of studying the effect of multipath on error performance in some of the simulations, we propose a simple channel model with $|\mathcal{L}|$ distinct delay paths, randomly chosen in the interval $[0, \tau_{\max}]$, with equal path gain. Each delay index can have a number of paths with different Doppler shifts uniformly distributed in the interval $[-\nu_{\max}, \nu_{\max}]$. Recall that $\mathcal{K}_\ell$ is the set containing the Doppler shifts of all paths with normalized delay ℓ, where $\ell \in \mathcal{L}$. The total number of paths $P = \sum_{\ell \in \mathcal{L}} |\mathcal{K}_\ell|$. Note that this scenario is unlikely to be found in any physical channel and is purely used to study the receiver performance under a simple set of controlled parameters. See MATLAB code 7 in Appendix C for generating the synthetic channel parameters for arbitrary delay and Doppler spread.

2.6 Bibliographical notes

We assume the reader is familiar with the basic notions of digital communications [1–3]. A more basic understanding of the exposition presented in this chapter can be found in [4–10]. Further details regarding the 3GPP standard channel models are available in [11]. General OFDM techniques for wireless communications were presented in [12]. OTFS modulation was first presented by Hadani et al. at the 2017 IEEE Wireless Communications and Networking Conference [13]. The channel representations of the different domains in various formats are discussed in [14–20].

References

[1] B. Sklar, F.J. Harris, Digital Communications: Fundamentals and Applications, Prentice-Hall, 1988.
[2] S. Benedetto, E. Biglieri, Principles of Digital Transmission with Wireless Applications, Springer US, 2002.
[3] J.G. Proakis, M. Salehi, Digital Communications, McGraw-Hill, 2008.
[4] B. Sklar, Rayleigh fading channels in mobile digital communication systems. I. Characterization, Philips Journal of Research 35 (7) (1997) 90–100.
[5] D. Tse, P. Viswanath, Fundamentals of Wireless Communication, 3rd edition, Cambridge University Press, 2005.
[6] A. Goldsmith, Wireless Communications, Cambridge University Press, 2005.
[7] G. Matz, F. Hlawatsch, Time-varying communication channels: fundamentals, recent developments, and open problems, in: 2006 14th European Signal Processing Conference, 2006, pp. 1–6.
[8] F. Hlawatsch, G. Matz, Wireless Communications over Rapidly Time-Varying Channels, 1st edition, Academic Press, Inc., USA, 2011.
[9] A.F. Molisch, Wireless Communications, second edition, John Wiley & Sons, 2011.
[10] P. Montezuma, F. Silva, R. Dinis, Frequency-Domain Receiver Design for Doubly Selective Channels, Taylor & Francis, 2017.

[11] European Telecommunications Standards Institute.
[12] Y.G. Li, G.L. Stuber, Orthogonal Frequency Division Multiplexing for Wireless Communications, Springer, 2006.
[13] R. Hadani, S. Rakib, M. Tsatsanis, A. Monk, A.J. Goldsmith, A.F. Molisch, R. Calderbank, Orthogonal time frequency space modulation, in: 2017 IEEE Wireless Communications and Networking Conference (WCNC), 2017, pp. 1–6.
[14] P. Raviteja, K.T. Phan, Y. Hong, E. Viterbo, Interference cancellation and iterative detection for orthogonal time frequency space modulation, IEEE Transactions on Wireless Communications 17 (10) (2018) 6501–6515, https://doi.org/10.1109/TWC.2018.2860011.
[15] K.R. Murali, A. Chockalingam, On OTFS modulation for high-Doppler fading channels, in: 2018 Information Theory and Applications Workshop (ITA), 2018, pp. 1–6.
[16] P. Raviteja, Y. Hong, E. Viterbo, E. Biglieri, Practical pulse-shaping waveforms for reduced-cyclic-prefix OTFS, IEEE Transactions on Vehicular Technology 68 (1) (2019) 957–961, https://doi.org/10.1109/TVT.2018.2878891.
[17] A. Farhang, A. RezazadehReyhani, L.E. Doyle, B. Farhang-Boroujeny, Low complexity modem structure for OFDM-based orthogonal time frequency space modulation, IEEE Wireless Communications Letters 7 (3) (2018) 344–347, https://doi.org/10.1109/LWC.2017.2776942.
[18] A. Rezazadehreyhani, A. Farhang, A. Ji, R.R. Chen, B. Farhang-Boroujeny, Analysis of discrete-time MIMO OFDM-based orthogonal time frequency space modulation, in: 2018 IEEE International Conference on Communications, 2018, pp. 1–6.
[19] W. Shen, L. Dai, J. An, P.Z. Fan, R.W. Heath, Channel estimation for orthogonal time frequency space (OTFS) massive MIMO, IEEE Transactions on Signal Processing 67 (16) (2019) 4204–4217, https://doi.org/10.1109/TSP.2019.2919411.
[20] T. Thaj, E. Viterbo, Y. Hong, Orthogonal time sequency multiplexing modulation: analysis and low-complexity receiver design, IEEE Transactions on Wireless Communications 20 (12) (2021) 7842–7855, https://doi.org/10.1109/TWC.2021.3088479.